SCIENTIFIC REPORTS

OPEN

SUBJECT AREAS:
CHEMICAL SYNTHESIS
HYDROLASES
MASS SPECTROMETRY
STRUCTURE-BASED DRUG DESIGN

Received
4 September 2012

Accepted
19 December 2012

Published
15 January 2013

Correspondence and requests for materials should be addressed to Y.-P.P. (pang@mayo.edu)

Novel Selective and Irreversible Mosquito Acetylcholinesterase Inhibitors for Controlling Malaria and Other Mosquito-Borne Diseases

Dengfeng Dou[1], Jewn Giew Park[1], Sandeep Rana[1], Benjamin J. Madden[2], Haobo Jiang[3] & Yuan-Ping Pang[1]

[1]Computer-Aided Molecular Design Laboratory, Mayo Clinic, Rochester, MN 55905, USA, [2]The Proteomics Core, Mayo Clinic, Rochester, MN 55905, USA, [3]Department of Entomology and Plant Pathology, Oklahoma State University, Stillwater, OK 74078, USA.

We reported previously that insect acetylcholinesterases (AChEs) could be selectively and irreversibly inhibited by methanethiosulfonates presumably through conjugation to an insect-specific cysteine in these enzymes. However, no direct proof for the conjugation has been published to date, and doubts remain about whether such cysteine-targeting inhibitors have desirable kinetic properties for insecticide use. Here we report mass spectrometric proof of the conjugation and new chemicals that irreversibly inhibited African malaria mosquito AChE with bimolecular inhibition rate constants (k_{inact}/K_I) of 3,604–458,597 $M^{-1}sec^{-1}$ but spared human AChE. In comparison, the insecticide paraoxon irreversibly inhibited mosquito and human AChEs with k_{inact}/K_I values of 1,915 and 1,507 $M^{-1}sec^{-1}$, respectively, under the same assay conditions. These results further support our hypothesis that the insect-specific AChE cysteine is a unique and unexplored target to develop new insecticides with reduced insecticide resistance and low toxicity to mammals, fish, and birds for the control of mosquito-borne diseases.

Malaria is a human disease caused by a protozoan parasite transmitted by mosquitoes[1] and has been a grave concern in human populations for ≥50,000 years[2,3]. According to the World Malaria Report 2011[4], approximately 3.3 billion people are at risk for contracting malaria, and an estimated 216 million cases led to nearly 655,000 deaths in 2010. Insecticides are a proven approach to controlling the disease. However, current insecticides are hampered by their toxicity to humans[5] and insecticide resistance[6]. There is an urgent need for novel insecticides to control the mosquitoes that transmit malaria and other mosquito-borne diseases such as West Nile virus infection[7] with reduced insecticide resistance and low toxicity to other species.

AChE is a hydrolase vital to the regulation of the neurotransmitter acetylcholine in mammals, fish, birds, and insects[8–10]. Its catalytic serine hydrolyzes acetylcholine at the bottom of its active site (Fig. 1). Current anticholinesterase insecticides work through covalent modification of this serine, thus disabling its catalytic function and incapacitating insects. However, because this serine is also ubiquitous in the AChEs of mammals and other species (Fig. 1), anticholinesterase insecticides are toxic to mammals, fish, and birds.

Interestingly, disease-transmitting mosquitoes such as the African malaria mosquito (*Anopheles gambiae* sensu stricto) and the common house mosquito (*Culex pipiens* L.) have two AChEs—Ace-paralogous AChE (AP-AChE) and Ace-orthologous AChE—both of which have an insect-specific cysteine residue near its active site[11]. Responsible for cholinergic functions[12–14], AP-AChE has an insect-specific cysteine located at the rim of its active site[11]. This cysteine has mutated to phenylalanine in the corresponding enzymes of mammals, fish, and birds[11] (Fig. 1). Because the AChEs of non-insect species lack this cysteine, cysteine-targeting AP-AChE inhibitors would have reduced off-species toxicity. Furthermore, these inhibitors have never been used as insecticides and therefore would have a lower propensity for inducing insecticide resistance relative to current anticholinesterase insecticides[11].

Following this reasoning, we developed methanethiosulfonate derivatives that selectively and irreversibly inhibit insect AP-AChEs presumably through conjugation to the insect-specific cysteine[12,15]. However, no direct proof of the conjugation of a sulfhydryl agent to the insect-specific cysteine in AP-AChE has been presented to date, and doubts have remained about whether the insect-specific cysteine is accessible for conjugation and whether cysteine-targeting AP-AChE inhibitors can be developed with kinetic properties comparable to those of

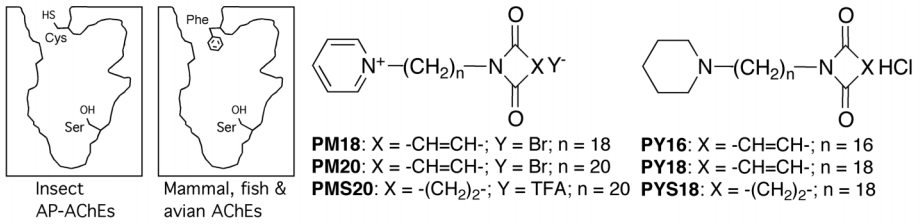

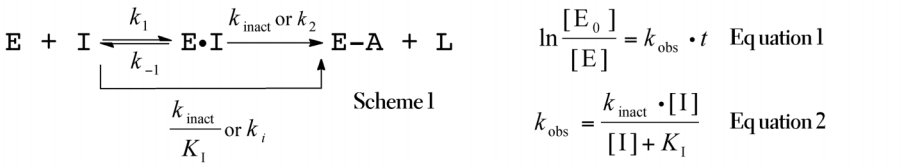

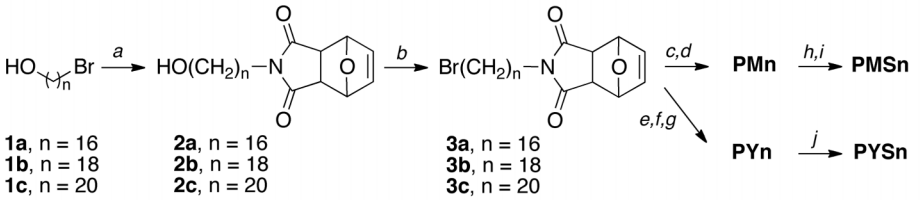

(*a*) 3a,4,7,7a-tetrahydro-1*H*-4,7-epoxyisoindole-1,3(2*H*)-dione, Cs_2CO_3, DMF, rt, 17-21 h, 96–100%; (*b*) NBS, PPh_3, THF, rt, 5 min, 73-75%; (*c*) pyridine (10-20 eq.), acetone, ↑↓, 17 h; (*d*) anisole, ↑↓, 15 min, 100%; (*e*) piperidine (5 eq), CH_3CN/DCM, rt, o/n; (*f*) anisole, ↑↓, 20 min; (*g*) HCl/MeOH, 94%; (*h*) PPh_3, MeOH, 75 °C, 4 h; (*i*) HPLC, 40-60%; (*j*) H_2/Pd-C, MeOH, rt, o/n, 100%.

Scheme 2

Figure 1 | New chemicals that target an insect-specific cysteine of AP-AChEs. Upper left panel: cross-section of the AP-AChE and AChE active sites showing the locations of the insect-specific cysteine and the corresponding residue in non-insect species; upper right panel: chemical structures of **PMn**, **PYn**, **PYS18**, and **PMS20**; middle panel: two-step quiescent affinity labeling mechanism for **PMn** and **PYn** and definition of kinetic parameters; lower panel: syntheses of **PMn**, **PYn**, **PYS18**, and **PMS20**. DCM: CH_2Cl_2; DMF: *N,N′*-dimethylformamide; NBS: *N*-bromosuccinimide; TFA: CF_3CO_2; THF: tetrahydrofuran; ↑↓: reflux.

insecticides. Here we report our redesigned inhibitors of *An. gambiae* sensu stricto AP-AChE (agAP-AChE) and direct proof for the conjugation of the new inhibitor to Cys286, the insect-specific cysteine in agAP-AChE. We also report kinetic data showing that the new inhibitors are superior to the insecticide paraoxon and discuss the feasibility of targeting the insect-specific cysteine to develop effective and environmentally safe insecticides.

Results

Design of agAP-AChE inhibitors. Encouraged by reports that small-molecule–conjugated fragments of cholinesterases can be detected using liquid chromatography mass spectrometry[16–22], we wanted to perform a mass spectrometric study of recombinant agAP-AChE[23] that was treated with our cysteine-targeting inhibitor before protein digestion to obtain direct proof of the conjugation of the sulfhydryl agent to Cys286. Our previously reported methanethiosulfonates form a disulfide bond with the insect-specific cysteine[12,15], and the methanethiosulfonate adducts are unstable in the presence of a disulfide-bond–cleavage agent during the digestion process. For this reason, we set out to develop maleimide-containing inhibitors that form a carbon-sulfur bond to Cys286, thereby their adducts are stable during the digestion process. We also sought to compare the kinetic properties of the new inhibitors with those of anticholinesterase insecticides.

As revealed by an agAP-AChE model refined using multiple molecular dynamics simulations (Protein Data Bank ID: 2AZG)[24], Cys286 is stabilized by aromatic residues via sulfur-aromatic interactions[25]. To react with Cys286, the cysteine-targeting inhibitor must have adequate affinity for the active site to accumulate a local concentration around Cys286 high enough to offset the sulfur-aromatic interaction. The inhibitor should also have adequate flexibility to satisfy the directional requirement for covalent bond formation.

Accordingly, we designed **PMn** and **PYn** (Fig. 1) as prototypic cysteine-targeting agAP-AChE inhibitors that were expected to follow the two-step quiescent affinity labeling mechanism[26] as depicted in Scheme 1 (Fig. 1). Specifically, these compounds were designed to react with Cys286 only after they reversibly bind in the vicinity of Cys286 with adequate affinity to impart target enzyme selectivity. The **PMn** series was inspired by a report that methylpyridinium binds well at the AChE active site[27]. The **PYn** series was designed purposely to have reduced affinity for the active site to investigate the effect of the inhibitor affinity on the inhibitor reactivity toward Cys286. The use of long alkylene chains in the prototypes was based on the chain-length–activity relationship of our reported irreversible AP-AChE inhibitors[12,15] and supported by 100 10-ns-long molecular dynamics simulations (each with unique initial velocities and a 1.0-fs time step) of agAP-AChE in reversible complex with **PM20** using an explicit water model[28–30]. These simulations predicted that **PM20** was capable of spanning the active site of agAP-AChE with its pyridinium group forming cation-pi interactions with Trp84, Tyr121, Tyr130, and Tyr328 and with its maleimide alkene carbon atom located 3.6 Å away from the sulfur atom of Cys286 (Fig. 2). To estimate the binding affinity of **PYn** and **PMn**, we also designed **PYS18** and **PMS20** whose maleimide is replaced with succinimide that cannot react with cysteine but is sterically almost identical to maleimide (Fig. 1). Notably, we made and tested **PMn** and **PYn** with n ranging from 10 to 22, but we report herein the representatives with n in the range of 16–20.

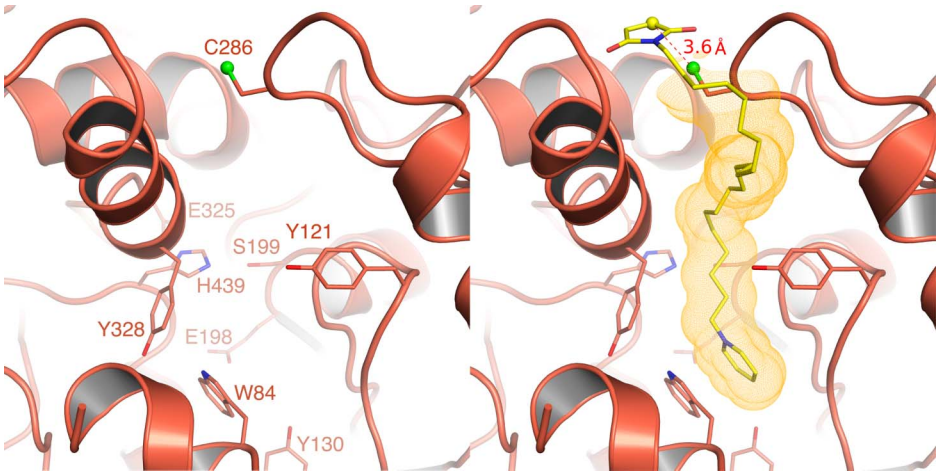

Figure 2 | Close-up view of agAP-AChE in reversible complex with PM20 predicted by microsecond molecular dynamics simulations. The nitrogen, oxygen, and sulfur atoms are in blue, red, and green, respectively. The carbon atoms in agAP-AChE and **PM20** are in tangerine and yellow, respectively. The mesh depicts the portion of **PM20** that is inserted in the active site of agAP-AChE. The simulation protocol is provided in the Supplementary Information.

Synthesis of agAP-AChE inhibitors. **PMn** and **PYn** were readily prepared in excellent yields following Scheme 2 (Fig. 1). The protected maleimide[31] was attached to an ω-substituted alkylene chain through reaction with $Br(CH_2)_nOH$. The hydroxyl group of the resulting intermediate was then substituted with bromide and subsequently converted to pyridinium or piperidine. Deprotection of the corresponding intermediate yielded **PMn** or **PYn**. Reduction of **PY18** and **PM20** gave **PYS18** and **PMS20**, respectively (Fig. 1).

Selective and irreversible inhibition of agAP-AChE. To determine whether **PMn** and **PYn** irreversibly inhibit recombinant agAP-AChE[23], we performed time-course experiments of AChE inhibition and found that **PMn** and **PYn** irreversibly inhibited recombinant agAP-AChE but not recombinant human AChE (hAChE). As shown in Figure 3, the irreversible inhibition is indicated by progressive inhibition over time, whereas reversible inhibition is evident from constant inhibition over time. As expected, the control inhibitor paraoxon irreversibly inhibited both enzymes, whereas **PMS20** and **PYS18** irreversibly inhibited neither (Fig. 3). The irreversible inhibition was then confirmed with dilution experiments[32] (Fig. 3), which determine the inhibitor dissociation from the enzyme upon dilution of the complex through measuring the reduction of the enzyme inhibition upon the dilution. If the complexation is irreversible, no complex dissociation occurs upon the dilution, and hence the percentage of enzyme inhibition remains constant after the dilution. Figure 3 demonstrates clearly that **PY18** and **PM20** irreversibly inhibited agAP-AChE but not hAChE.

Proof of the Cys286 conjugation in agAP-AChE. To prove that the observed selective and irreversible inhibition of agAP-AChE by **PM20** is due to the conjugation of the inhibitor to Cys286, we performed nano-flow liquid-chromatography electrospray ionization tandem mass spectrometry (nanoLC–ESI-MS/MS) analysis[33] on recombinant agAP-AChE[23] that was treated with **PM20** followed by protein digestion. We identified a doubly-charged ion from a high-resolution Orbitrap survey scan with the monoisotopic mass of 1082.6122 (Fig. 4). The mass of this ion was within 0.2 parts per million (ppm) of the calculated mass over charge ratios (*m/z*) of 1082.6120 (82.6%) and 1083.1137 (100.0%) for $[GIC^{PM20}EFPFVPVVDGAFL+H]^{+2}$, a fragment of agAP-AChE. C^{PM20} is Cys286 conjugated with **PM20** via Michael addition[34], and two formal charges reside on the **PM20** pyridinium ring and the *N*-terminus.

The conjugated peptide identification was then confirmed with the tandem mass spectrometry showing the b- and y-type ions[35] resulting from collision-induced fragmentations of $[GIC^{PM20}EFPFVPVVDGAFL+H]^{+2}$ in the linear ion trap component of the spectrometer. It has been reported that the b_n ions, which are generated by collision and display cleavage at the peptide bond of the n^{th} residue counting from the *N*-terminus, exist in a linear peptidic form with a *C*-terminal oxazolone[36–41], in a cyclic peptidic form resulting from the reaction between the *N*-terminus and the oxazolone group[41–47] (Fig. 4), or as a mixture of the two[40]. Smaller b ions ($n = 2$ or 3) reportedly adopt the linear form exclusively, whereas b_8 ion adopts exclusively the cyclic form[40]. The masses of both linear and cyclic forms are one hydrogen atom less than that of the corresponding linear peptide without the oxazolone group. In this study, we were interested in the masses of the b_n ions rather than their structures and therefore calculated the b_n ($n > 3$) ion masses using the cyclic form. The calculated b-ion *m/z* values of cyclo$(GIC^{PM20}E)^+$, cyclo$(GIC^{PM20}EF)^+$, cyclo$(GIC^{PM20}EFP)^+$, cyclo$(GIC^{PM20}EFPF)^+$, cyclo$(GIC^{PM20}EFPFV)^+$, cyclo$(GIC^{PM20}EFPFVPV)^+$, cyclo$(GIC^{PM20}EFPFVPVV)^+$, and cyclo$(GIC^{PM20}EFPFVPVVD)^+$ were 857.52, 1004.59, 1101.64, 1248.71, 1347.78, 1543.90, and 1643.97, respectively. These values corresponded well with the observed b ions (Fig. 4). For the y_n ions that have breakage at the peptide bond of the n^{th} residue counting from the *C*-terminus, the calculated y ion *m/z* values of $[P_{292}VVDGAFL+H]^+$ and $[P_{289}FVPVVDGAFL+H]^+$ were 817.45 and 1160.64, respectively, which were in excellent agreement with the observed y ions (Fig. 4). The conjugated peptide identification was also confirmed with the tandem mass spectra showing the same b- and y-type ions resulting from collision-induced fragmentations of $[GIC^{PM20}EFPFVPVVDGAFL+H]^{+2}$ and the **PM20**-conjuated synthetic peptide of the same sequence (data not shown).

Of eight cysteine residues in our recombinant agAP-AChE[23], the nanoLC–ESI-MS/MS analysis showed that only Cys286 was conjugated with **PM20** and that others were identified as carboxamidomethyl cysteine due to reduction of the three intramolecular and one intermolecular disulfide bonds of the recombinant enzyme and subsequent alkylation of the resulting thiols during the enzyme digestion process. It is known that only Cys, Lys, and His react with maleimides[48,49]. The agAP-AChE model[24] shows that the active-site and peripheral-site regions contain only one His residue (His439) and no Lys residue. The nanoLC–ESI-MS/MS analysis did not identify any His439-containing fragment carrying the **PM20** adduct. These results provide direct proof for the conjugation of **PM20** to the insect-specific cysteine in agAP-AChE.

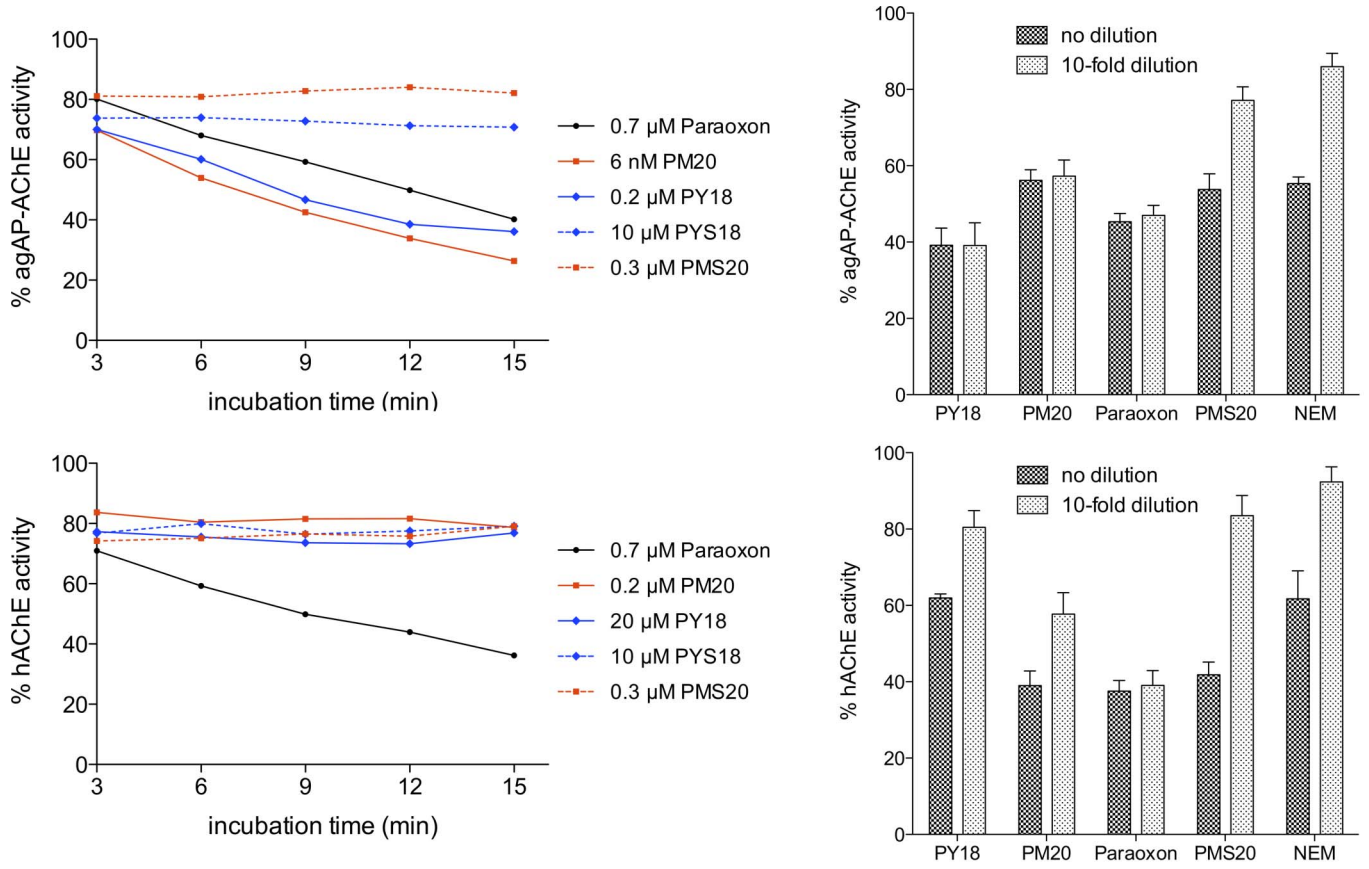

Figure 3 | Time-course and dilution experiments for the inhibition of agAP-AChE and hAChE by PY18, PM20, PMS20, paraoxon, and NEM. % enzyme activity: the enzyme activity compared to that without inhibitor treatment. Before the 10-fold dilution, the concentrations of **PY18**, **PM20**, **PMS20**, paraoxon, and NEM were 0.1, 0.001, 1.67, 0.2, and 100 μM for the agAP-AChE inhibition assays and 6.67, 0.5, 0.833, 0.2, and 100 μM for the hAChE inhibition assays, respectively.

Kinetic studies of AP-AChE inhibitors. After confirming the mechanism for the selective and irreversible inhibition of agAP-AChE by **PMn**, we determined bimolecular inhibition rate constants (k_{inact}/K_I or k_i) and pseudo-unimolecular inhibition rate constants (k_{inact} or k_2) of our irreversible inhibitors and the control inhibitor paraoxon (Fig. 5 and Table 1), using nonlinear regression fitting analysis[50] according to Equations 1 and 2 (Fig. 1). We found that the bimolecular inhibition rate constants (k_{inact}/K_I or k_i) for inhibiting agAP-AChE and hAChE by paraoxon were 1,915 and 1,507 $M^{-1}sec^{-1}$, respectively, at high paraoxon concentrations of 333–2000 nM with incubation times of 15 minutes or less (Fig. 5 and Table 1). These values changed to 9,862 and 10,013 $M^{-1}sec^{-1}$, respectively, at low paraoxon concentrations of 17–100 nM with incubation times of 75 minutes or less. These results are consistent with reports that the kinetics of AChE inhibition by paraoxon is concentration dependent[51–53]. Our bimolecular inhibition rate constants measured at low paraoxon concentrations are comparable to those reported for agAP-AChE[23] and mammalian AChEs[51–55].

Because we were interested in knowing how quickly our compounds inhibited agAP-AChE and the inhibitory potency of the redesigned inhibitors relative to that of paraoxon, we measured the kinetic data of **PMn** and **PYn** over time courses of ≤15 minutes. In this context, we found that **PMn** and **PYn** irreversibly inhibited agAP-AChE with pseudo-unimolecular inhibition rate constants of 10–56 hr^{-1} and bimolecular inhibition rate constants of 3,013–458,597 $M^{-1}sec^{-1}$ (Table 1 and Fig. 5). We also found that **PMn** and **PYn** reversibly inhibited hAChE with equilibrium dissociation constants (K_i) of 0.12–20.37 μM (Table 1 and Fig. 6) and that **PYS18** and **PMS20** reversibly inhibited insect and human enzymes with K_i values of 26.18 and 0.42 μM, respectively (Table 1 and Fig. 6).

In addition, as shown in Figure 5, the observed inhibition rate constants (k_{obs}) of **PMn** and **PYn** were nonlinear functions of inhibitor concentration ([I]), indicating that the designed inhibitors indeed followed the two-step quiescent affinity labeling mechanism rather than the one-step nonspecific affinity labeling mechanism characterized by a linear relationship between k_{obs} and [I][26].

Effect of inhibitor affinity on inhibitor reactivity. To evaluate the prospect of using cysteine-targeting inhibitors as insecticides with consideration to their potential reactions with off-target cysteines, we studied the effect of inhibitor affinity on inhibitor reactivity toward the cysteine. As shown in Figure 7, treating agAP-AChE with 50 μM *N*-ethylmaleimide (NEM) immediately resulted in 36 ± 2% inhibition of the enzyme activity, and extending the treatment for 30 minutes slightly increased the inhibition to 40 ± 1%, whereas treating agAP-AChE with a combination of 50 μM NEM and 6.7 nM **PM20** for 30 minutes decreased the enzyme activity by 94 ± 3%. In addition, Figure 3 shows that, when agAP-AChE was incubated with 100 μM NEM for 30 minutes, 45 ± 2% of the enzyme activity was inhibited; when the incubation solution was diluted by 10-fold, the enzyme inhibition was reduced to 14 ± 4%. These results demonstrate the inability of NEM to irreversibly inhibit agAP-AChE. However, the inability of NEM to irreversibly inhibit agAP-AChE does not imply that NEM cannot react with Cys286, because NEM lacks a long chain that can physically block the active site. Nevertheless, when agAP-AChE was incubated with 50 μM NEM, only 40 ± 1% of the enzyme activity was inhibited; when the

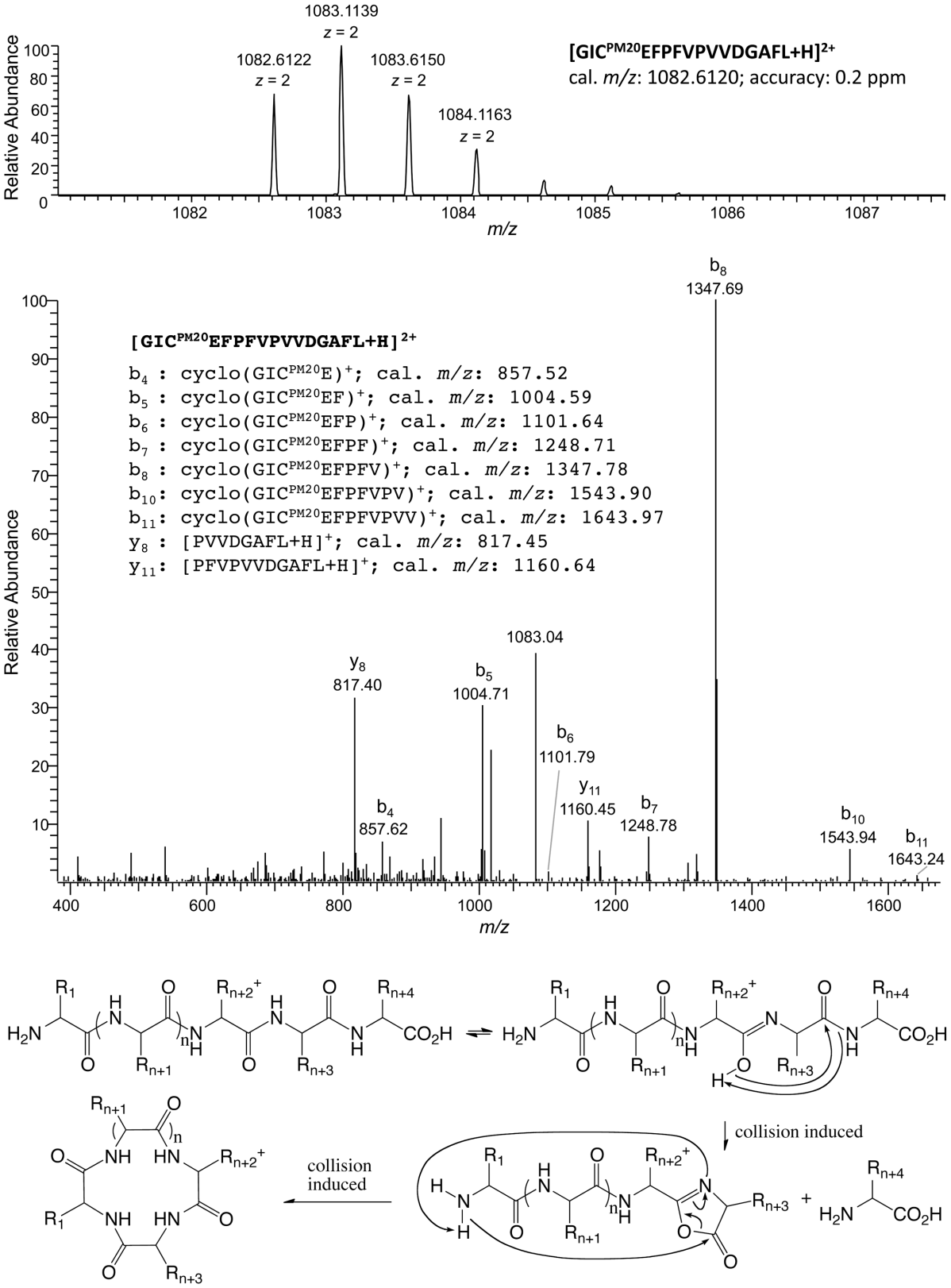

Figure 4 | Mass spectrometric proof of the conjugation of PM20 to Cys286 in agAP-AChE. Upper panel: high-resolution Fourier transform mass spectrometry survey scan of the $[M+H]^{+2}$ ion (*m/z* of 1082.6122) corresponding to the **PM20**-labeled fragment of agAP-AChE with calculated (cal.) *m/z* of 1082.6120. Middle panel: supporting tandem mass spectrum showing the observed b- and y-type ions resulting from fragmentations of the $[M+H]^{2+}$ ion. Lower panel: mechanisms for the oxazolone formation and b-ion cyclization.

incubation solution was then treated with 6.7 nM **PM20** for 30 minutes, 96 ± 4% of the enzyme activity was inhibited (Fig. 7). These results indicate that 50 μM NEM cannot react with Cys286. Otherwise, Cys286 would be blocked by NEM and the subsequent 30-minute treatment with 6.7 nM **PM20** would not lead to the 96 ± 4% enzyme inhibition (Fig. 7). We also found that 1-ethylpyrrolidine-2,5-dione, a close analog of NEM, did not irreversibly or reversibly inhibit agAP-AChE and hAChE at

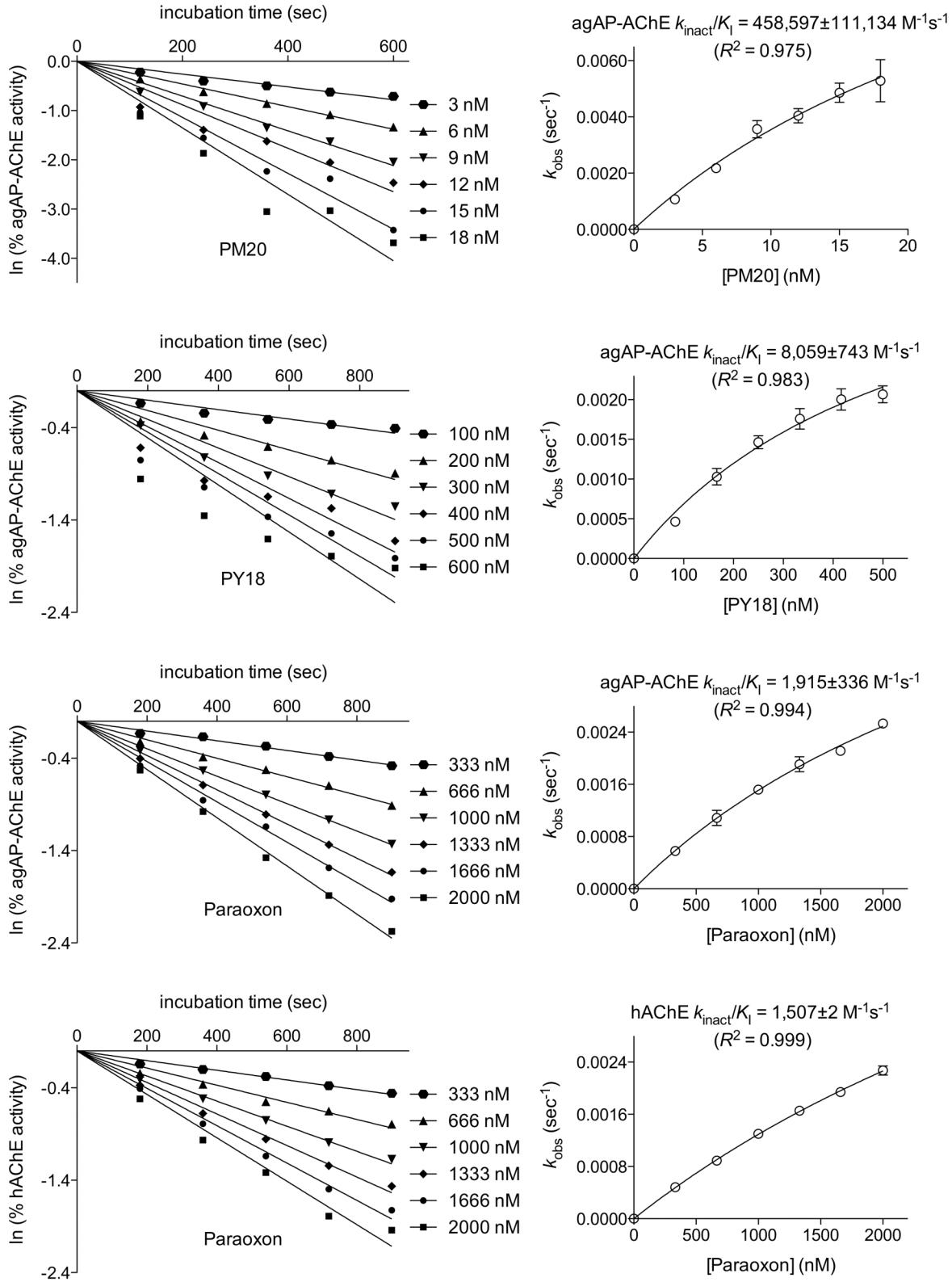

Figure 5 | Progressive AChE inhibition as a function of time and inhibitor concentration indicating the two-step quiescent affinity labeling mechanism for the test inhibitors. % enzyme activity: the enzyme activity compared to that without inhibitor treatment. Left: linear plots of natural log of % AChE activity versus time in second at different inhibitor concentrations; right: nonlinear plots of the observed inhibition rate in 1/second versus inhibitor concentration in nanomolar.

inhibitor concentrations up to 10 mM (data not shown), indicating that NEM has much lower affinity for agAP-AChE than **PMn** or **PYn**. These studies reveal the correlation between the low affinity of NEM for agAP-AChE and its inability to react with Cys286. More importantly, these studies demonstrate that the markedly increased reactivity of the maleimide in **PM20** toward Cys286 is due to the affinity gained from attaching maleimide to *N*-alkylpyridinium.

Table 1 | Irreversible and Reversible Inhibition of agAP-AChE and hAChE

Irreversible Inhibition				
Inhibitor	Incubation (min)	k_{inact} (hr^{-1})[a]	K_I (μM)[b]	k_{inact}/K_I ($M^{-1}s^{-1}$)[c]
		agAP-AChE		
PY16 (100–600 nM)	≤15	15.4 ± 1.5	1.19 ± 0.13	3604 ± 45
PY18 (100–600 nM)	≤15	16.7 ± 0.4	0.58 ± 0.04	8059 ± 743
PM18 (4–26 nM)	≤15	10.4 ± 0.9	0.013 ± 0.001	230155 ± 26492
PM20 (3–18 nM)	≤15	56.3 ± 22.4	0.034 ± 0.017	458597 ± 111134
Paraoxon (333–2000 nM)	≤15	25.6 ± 5.6	3.71 ± 1.24	1915 ± 336
Paraoxon (17–100 nM)	≤75	10.3 ± 0.4	0.289 ± 0.009	9862 ± 96
		hAChE		
Paraoxon (333–2000 nM)	≤15	32.7 ± 2.7	6.03 ± 0.49	1507 ± 2
Paraoxon (17–100 nM)	≤75	5.8 ± 1.2	0.161 ± 0.048	10,013 ± 721

Reversible Inhibition			
	K_i (μM)[d]		
	hAChE	*ag*AP-AChE	Selectivity for insect
PY16	11.75 ± 0.51	—	—
PY18	20.37 ± 1.54	—	—
PM18	0.12 ± 0.01	—	—
PM20	0.36 ± 0.01	—	—
PMS20	0.42 ± 0.02	0.40 ± 0.04	1.1
PYS18	17.91 ± 0.02	26.18 ± 1.57	0.7

[a]k_{inact}: pseudo-unimolecular inhibition rate constant; [b]K_I: the inhibitor concentration that yields a rate of inactivation that is equal to a half of k_{inact}; [c]k_{inact}/K_I: bimolecular inhibition rate constant; [d]K_i: equilibrium dissociation constant.

Discussion

The present studies show that **PMn** and **PYn** can selectively and irreversibly inhibit agAP-AChE. The mechanism for the irreversible inhibition is now known due to the conjugation of the inhibitor to Cys286, the insect-specific cysteine in agAP-AChE, according to the nanoLC–ESI-MS/MS analysis. The mass spectroscopic data are consistent with our previous reports[12,15] that the irreversible inhibition of insect AChEs by a methanethiosulfonate could be partially restored by β-mercaptoethanol that cleaves in theory the disulfide bonds in the enzymes (leading to enzyme inhibition) and the disulfide bond of the methanethiosulfonate to Cys286 in agAP-AChE or Cys289 in greenbug AP-AChE (leading to enzyme reactivation). Given the experimental data of our previous and present studies, we conclude that the insect-specific cysteine in AP-AChE is accessible for conjugation with high-affinity and flexible sulfhydryl agents and that such conjugation can lead to the selective and irreversible inhibition of AP-AChEs.

Furthermore, the present work demonstrates the correlation between the reactivity of the cysteine-targeting inhibitors and their binding affinity. Because the bimolecular inhibition rate constant (k_{inact}/K_I) of **PM20** is 239-fold higher than that of paraoxon (Table 1), structural modification of **PM20** to change its K_i for agAP-AChE from the present 400 nM to 4 nM can, in theory, yield a new inhibitor with k_{inact}/K_I equivalent to that of paraoxon but with an electrophile that can be ~24,000-fold less reactive than maleimide. Given the report that the AChE inhibitor K_i can be improved to 33 fM[56], the expectation that the K_i of **PM20** can be improved to 4 nM is conservative. The replacement of maleimide with such a weak electrophile would prevent the new inhibitor from reacting with off-target cysteines. For that reasons, we believe that the insect-specific AChE cysteine is a unique and unexplored target to develop new insecticides with reduced insecticide resistance and low toxicity to mammals, fish, and birds for the control of malaria and other mosquito-borne diseases.

Methods

Materials. Acetylthiocholine (ATCh) and Triton X-100 were purchased from ACROS (Morris Plains, NJ), and 5,5′-dithiobis-2-nitrobenzoate (DTNB) was ordered from Sigma-Aldrich (St. Louis, MO). Recombinant agAP-AChE with a specific activity of ≥461 U/mg (36.67 ng/μL) in the presence of 5% glycerol was made according to a published protocol[23]. Recombinant hAChE with a specific activity of ≥1500 U/mg was purchased as a lyophilized powder from Sigma-Aldrich (catalog number: C1682) and dissolved in 50 mM phosphate buffer (pH 8.0) containing 0.1% Triton X-100 as a stock solution. Peptide *GICEFPFVPVVDGAFL* was purchased from GenScript (Piscataway, NJ).

General description of chemical synthesis. ^{1}H NMR (400 MHz) and ^{13}C NMR (100 MHz) spectra were recorded on a Mercury 400 spectrometer from Varian (Palo Alto, CA). Chemical shifts are reported in ppm using the solvent peak as an internal standard. Data are reported as follows: chemical shift, multiplicity (s = singlet, d = doublet, t = triplet, and m = multiplet), coupling constant, and integration. Low-resolution mass spectra (LRMS) were recorded using either a Hewlett Packard 5973 Mass Spectrometer with SIS Direct Insertion Probe (Palo Alto, CA) or a Waters ZQ 2000 Mass Spectrometer (Milford, MA). High-resolution mass spectra (HRMS) were obtained on a Bruker BioTOF II ESI. IR spectra were obtained on a ThermoNicolet Avatar 370 FT-IR (Waltham, MA) using a KBr pellet. A Biotage SP-1 (Charlotte, NC) was used for medium pressure liquid chromatography (MPLC) purification using silica gel as the packing material. 16-Bromo-1-hexadecanol (**1a**) was purchased from Astatech, Inc. (Bristol, PA), octadecanedioic acid and eicosanedioic acid from TCI America (Portland, OR), respectively, and used as received. Anhydrous tetrahydrofuran (THF), $LiAlH_4$, and 48% hydrobromic acid were purchased from Sigma-Aldrich (St. Louis, MO). *N*-Bromosuccinimide (NBS) was purchased from Fisher Scientific (Pittsburgh, PA), and recrystallized from water before use.

1-(16-Hydroxyhexadecyl)-3a,4,7,7a-tetrahydro-1*H*-4,7-epoxyisoindole-1,3(2*H*)-dione (2a). To a stirred solution of 16-bromo-1-hexadecanol (**1a**, 0.32 g, 1.00 mmol) in DMF (10 mL) at room temperature was added 3a,4,7,7a-tetrahydro-1*H*-4,7-epoxyisoindole-1,3(2*H*)-dione (0.16 g, 1.00 mmol) then followed by cesium carbonate (0.49 g, 1.50 mmol). The mixture was stirred at room temperature for 18 hours. Diluted with water (10 mL), extracted with methylene chloride (10 mL), dried ($MgSO_4$), filtered, and then concentrated, further dried under high vacuum to give 0.41 g (100%) of **2a** as a white powder, mp 84–86°C;^{1}H NMR (400 MHz, $CDCl_3$) δ 6.49 (s, 2H), 5.24 (s, 2H), 3.61 (t, J = 6.6 Hz, 2H), 3.43 (t, J = 7.4 Hz, 2H), 2.81 (s, 2H), 1.56–1.51 (m, 5H), and 1.31–1.22 (m, 24H); ^{13}C NMR (100 MHz, $CDCl_3$) δ 176.56, 136.76, 81.11, 63.28, 47.60, 39.27, 33.03, 29.85, 29.83, 29.75, 29.66, 29.34, 27.82, 26.91, and 25.96; IR (KBr) ν 3422, 3363, 2925, 2849, 1698, and 879 cm^{-1}; LRMS (EI) m/z 338 (100%, $[M\text{-}C_4H_4O]^+$); HRMS (ESI) m/z 338.2692 ($[M\text{-}C_4H_4O+H]^+$, $C_{20}H_{36}NO_3^+$ requires 338.2695). Anal. calcd for $C_{24}H_{39}NO_4 \cdot 0.5H_2O$: C, 69.53; H, 9.72; N, 3.38. Found: C, 69.67; H, 9.36; N, 3.38.

1-(18-Hydroxyoctadecyl)-3a,4,7,7a-tetrahydro-1*H*-4,7-epoxyisoindole-1,3(2*H*)-dione (2b). Compound **2b** was synthesized from **1b**, which was prepared according to a published protocol[57], in 96% yield in the same manner as the synthesis of **2a**,

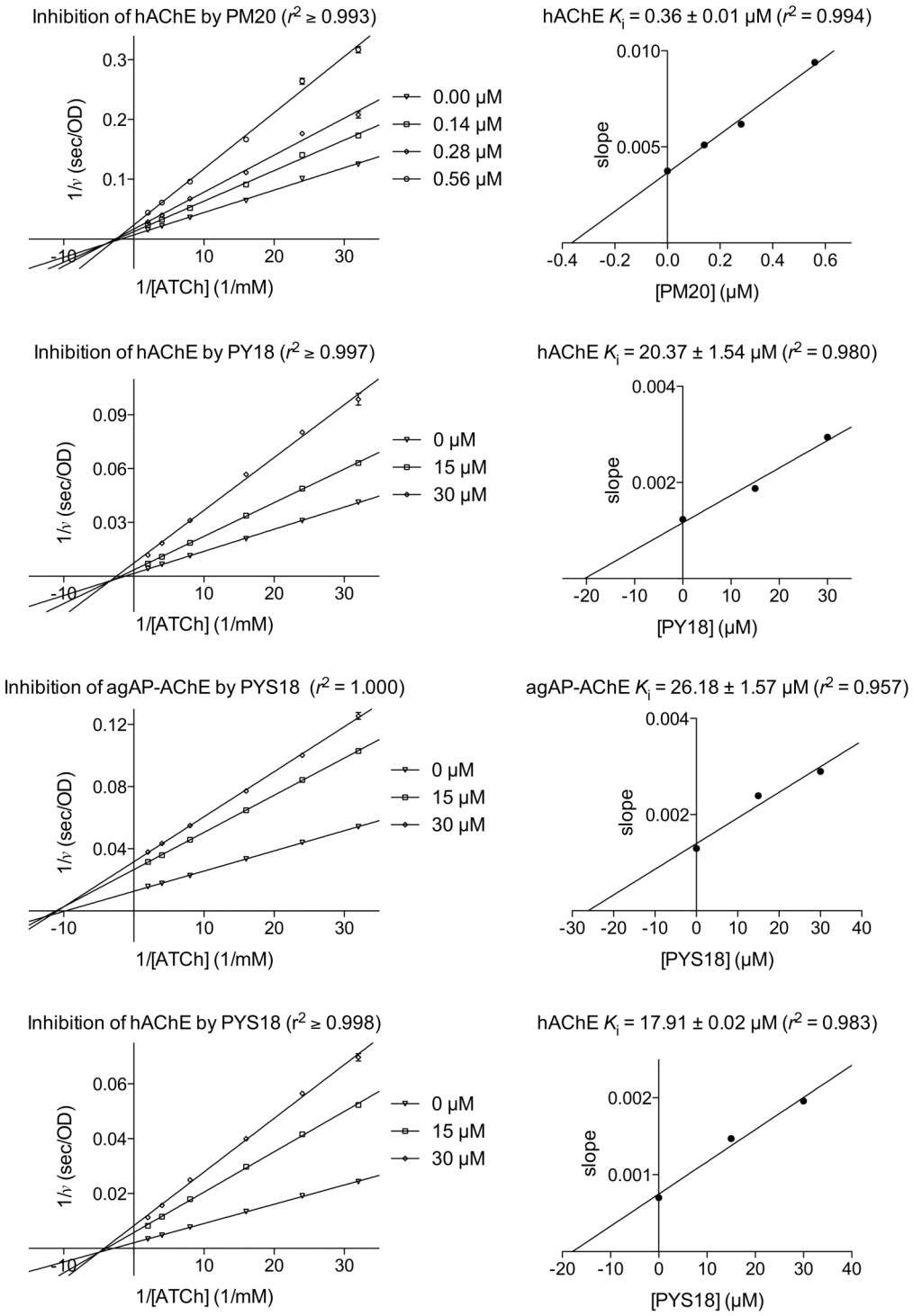

Figure 6 | Determination of equilibrium dissociation constants (K_i). Left: reciprocal hydrolysis rate ($1/v$ in second per optical density) was plotted against reciprocal substrate concentration (1/[ATCh] in 1/mM) in the absence and presence of an inhibitor at varying concentrations; right: the slope of the double reciprocal plot was plotted against inhibitor concentration ([I] in μM). K_i was obtained from the negative x intercept of the slope replot.

mp 84–86°C; ^{1}H NMR (400 MHz, $CDCl_3$) δ 6.49 (s, 2H), 5.24 (s, 2H), 3.61 (t, J = 6.6 Hz, 2H), 3.43 (t, J = 7.4 Hz, 2H), 2.81 (s, 2H), 1.66 (brs, 1H), 1.56–1.48 (m, 4H), and 1.31–1.22 (m, 28H); ^{13}C NMR (100 MHz, $CDCl_3$) δ 176.57, 136.76, 81.11, 63.26, 47.59, 39.26, 33.03, 29.88, 29.83, 29.76, 29.68, 29.67, 29.35, 27.82, 26.91, and 25.97; IR (KBr) ν 3426, 2923, 2848, 1698, and 879 cm^{-1}; LRMS (EI) m/z 365 (100%, $[M\text{-}C_4H_4O]^+$); HRMS (ESI) m/z 388.2816 ($[M\text{-}C_4H_4O+Na]^+$, $C_{22}H_{39}NO_3Na^+$ requires 388.2828). Anal. calcd for $C_{26}H_{43}NO_4 \cdot H_2O$: C, 69.14; H, 10.04; N, 3.10. Found: C, 70.88; H, 10.16; N, 3.10.

1-(20-Hydroxyeicosyl)-3a,4,7,7a-tetrahydro-1*H*-4,7-epoxyisoindole-1,3(2*H*)-dione (2c). Compound **2c** was synthesized from **1c**, which was prepared according to a published protocol[57], in 100% yield in the same manner as the synthesis of **2a**, mp 79–82°C;^{1}H NMR (400 MHz, $CDCl_3$) δ 6.50 (s, 2H), 5.25 (s, 2H), 3.63 (t, J = 6.6 Hz, 2H), 3.45 (t, J = 7.4 Hz, 2H), 2.82 (s, 2H), 1.57–1.52 (m, 5H), and 1.33–1.23 (m, 32H); ^{13}C NMR (100 MHz, $CDCl_3$) δ 176.56, 136.77, 81.12, 63.33, 47.61, 39.28, 33.04, 29.90, 29.85, 29.78, 29.70, 29.67, 29.36, 27.84, 26.92, and 25.97; IR (KBr) ν 3430, 2920, 2849, 1700, and 878 cm^{-1}; LRMS (EI) m/z 393 (100%, $[M\text{-}C_4H_4O]^+$); HRMS (ESI) m/z 484.3414 ($[M+Na]^+$, $C_{28}H_{47}NO_4Na^+$ requires 484.3403). Anal. calcd for $C_{28}H_{47}NO_4 \cdot H_2O$: C, 70.11; H, 10.30; N, 2.92. Found: C, 70.73; H, 10.36; N, 2.71.

1-(16-Bromohexadecyl)-3a,4,7,7a-tetrahydro-1*H*-4,7-epoxyisoindole-1,3(2*H*)-dione (3a). NBS (89 mg, 0.50 mmol) was added into a stirred solution of **2a** (0.20 g,

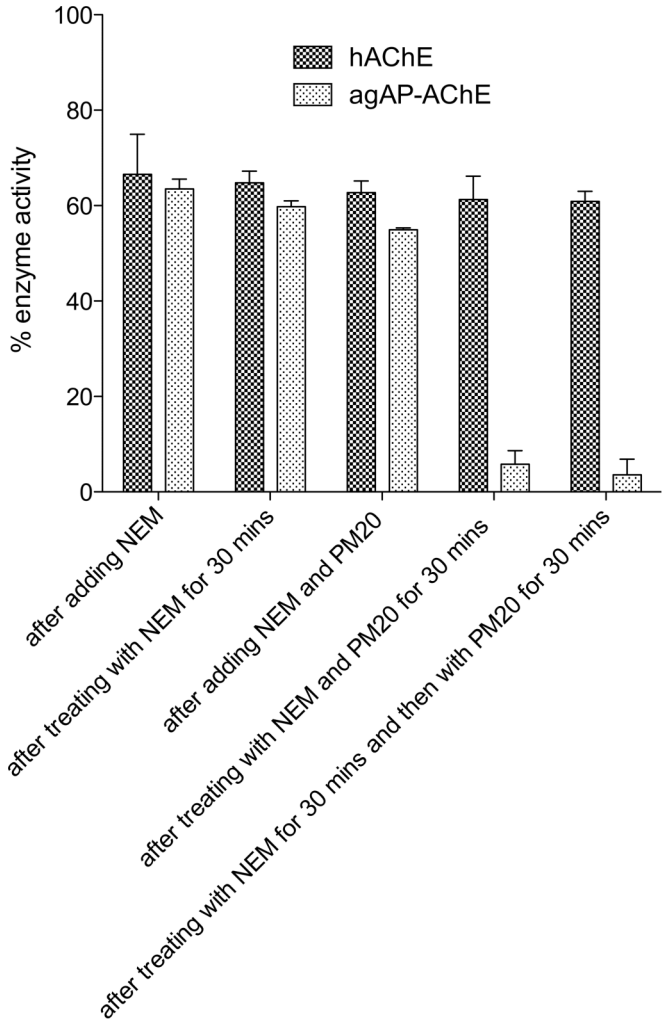

Figure 7 | Effects of 50 μM NEM and 6.7 nM PM20 on agAP-AChE and hAChE activities. % enzyme activity: the enzyme activity compared to that without inhibitor treatment.

0.50 mmol) and triphenylphosphine (0.13 g, 0.50 mmol) in dry THF (10 mL) at room temperature. After 5 minutes, water (10 mL) was added, layers were separated, the aqueous layer was extracted with methylene chloride (2 × 10 mL), organic layers were combined, dried ($MgSO_4$), filtered, and then purified by MPLC (silica gel, EtOAc:Hex = 1:4) to give 0.17 g (75%) of **3a** as a white solid, mp 76–78°C; ^{1}H NMR (400 MHz, $CDCl_3$) δ 6.50 (s, 2H), 5.25 (s, 2H), 3.45 (t, J = 7.4 Hz, 2H), 3.40 (t, J = 6.9 Hz, 2H), 1.88–1.81 (m, 2H), 1.57–1.52 (m, 2H), 1.43–1.41 (m, 2H), and 1.39–1.23 (m, 24H); ^{13}C NMR (100 MHz, $CDCl_3$) δ 176.47, 136.73, 81.08, 47.58, 39.19, 34.29, 33.03, 29.83, 29.80, 29.73, 29.64, 29.31, 28.96, 28.38, 27.78, and 26.86; IR (KBr) ν 2919, 2848, 1704, 1400, and 876 cm^{-1}; LRMS (EI) m/z 399 (100%, $[M\text{-}C_4H_4O]^+$). Anal. calcd for $C_{24}H_{38}BrNO_3$: C, 61.53; H, 8.18; N, 2.99. Found: C, 61.10; H, 8.46; N, 2.94.

1-(18-Bromooctadecyl)-3a,4,7,7a-tetrahydro-1*H*-4,7-epoxyisoindole-1,3(2*H*)-dione (3b). Compound **3b** was synthesized from **2b** (75% yield) in the same manner as the synthesis of **3a**, mp 66−69°C;^{1}H NMR (400 MHz, $CDCl_3$) δ 6.51 (s, 2H), 5.26 (s, 2H), 3.45 (t, J = 7.4 Hz, 2H), 3.40 (t, J = 6.9 Hz, 2H), 2.82 (s, 2H), 1.86–1.81 (m, 2H), 1.43–1.39 (m, 2H), and 1.27–1.23 (m, 28H); ^{13}C NMR (100 MHz, $CDCl_3$) δ 176.53, 136.76, 81.12, 47.60, 39.26, 34.35, 33.07, 29.91, 29.86, 29.78, 29.70, 29.67, 29.35, 29.00, 28.41, 27.83, and 26.91; IR (KBr) ν 2919, 2848, 1704, 1401, and 876 cm^{-1}; LRMS (EI) m/z 495 (2%, $[M]^+$), 429 (100%, $[M\text{-}C_4H_4O]^+$); HRMS m/z 427.2066 ($[M\text{-}C_4H_4O]^+$, $C_{22}H_{38}BrNO_2^+$ requires 427.2086). Anal. calcd for $C_{26}H_{42}BrNO_3$: C, 62.89; H, 8.53; N, 2.82. Found: C, 62.69; H, 8.90; N, 2.70.

1-(20-Bromoeicosyl)-3a,4,7,7a-tetrahydro-1*H*-4,7-epoxyisoindole-1,3(2*H*)-dione (3c). Compound **3c** was synthesized from **2c** (73% yield) in the same manner as the synthesis of **3a**, mp 81–83°C; ^{1}H NMR (400 MHz, $CDCl_3$) δ 6.50 (s, 2H), 5.26 (s, 2H), 3.45 (t, J = 7.4 Hz, 2H), 3.40 (t, J = 6.8 Hz, 2H), 2.82 (s, 2H), 1.88–1.81 (m, 2H) 1.43–1.39 (m, 2H), and 1.27–1.23 (m, 32H); ^{13}C NMR (100 MHz, $CDCl_3$) δ 176.49, 136.81, 136.64, 81.25, 80.96, 47.83, 47.37, 39.25, 34.28, 33.06, 29.83, 29.76, 29.67, 29.34, 28.98, 28.40, 27.83, and 26.90; IR (KBr) ν 2913, 2844, 1704, 1401, and 870 cm^{-1}; LRMS (EI) m/z 523 (6%, $[M]^+$), and 455 (77%, $[M\text{-}C_4H_4O]^+$). Anal. calcd for $C_{28}H_{46}BrNO_3$: C, 64.11; H, 8.84; N, 2.67. Found: C, 64.10; H, 9.24; N, 2.59.

1-(16-(Piperidin-1-yl)hexadecyl)-1*H*-pyrrole-2,5-dione hydrochloride (PY16). A solution of compound **3a** (150 mg, 0.32 mmol) and piperidine (150 μL, 1.50 mmol) in acetonitrile (10 mL) and methylene chloride (5 mL) was stirred at room temperature overnight. The solvent was removed and the crude product was purified using MPLC (silica gel/DCM/MeOH) to give the intermediate as a white solid. The intermediate was treated with 0.5 mL of 3 M methanolic HCl and then evaporated to dryness. The residue was heated to reflux in anisole (3 mL) for 20 min. The solvent was removed, yielding pure **PY16** as an off-white solid (128 mg, 93% yield), mp 118–120°C; ^{1}H NMR (400 MHz, $CDCl_3$) δ 10.92 (s, 1H), 6.63 (s, 2H), 3.49–3.42 (m, 2H), 3.42 (t, J = 7.2 Hz, 2H), 2.92–2.85 (m, 2H), 2.75–2.63 (m, 2H), 2.31–2.18 (m, 2H), 1.87–1.76 (m, 4H), 1.53–1.45 (m, 2H), 1.30–1.13 (m, 26H); ^{13}C NMR (100 MHz, $CDCl_3$) 171.09, 134.25, 57.78, 53.30, 38.09, 29.78, 29.73, 29.70, 29.64, 29.57, 29.29, 29.22, 28.72, 27.06, 26.91, 23.71, 22.74, and 22.23; IR (KBr) ν 3447, 2921, 2849, 1699 cm^{-1}; LRMS (ESI) m/z 405.28 (100%, $[M+H]^+$); HRMS (ESI) m/z 405.3469 ($[M+H]^+$, $C_{25}H_{45}N_2O_2^+$ requires 405.3481). Anal. calcd for $C_{25}H_{45}ClN_2O_2$: C, 65.40; H, 10.32; N, 6.10. Found: C, 65.69; H, 10.51; N, 6.07.

1-(18-(Piperidin-1-yl)octadecyl)-1*H*-pyrrole-2,5-dione hydrochloride (PY18). Compound **PY18** was synthesized from **3b** (71% yield) in the same manner as the synthesis of **PY16**, mp 129−131°C; ^{1}H NMR (400 MHz, $CDCl_3$) δ 11.58 (s, 1H), 6.65 (s, 2H), 3.60–3.45 (m, 2H), 3.49 (t, J = 7.2 Hz, 2H), 2.95–2.85 (m, 2H), 2.70–2.55 (m, 2H), 2.40–2.25 (m, 2H), 1.95–1.80 (m, 8H), 1.60–1.50 (m, 2H), and 1.35–1.18 (m, 26H); ^{13}C NMR (100 MHz, $CDCl_3$) 171.16, 134.28, 58.07, 53.59, 38.17, 29.88, 29.85, 29.80, 29.78, 29.72, 29.64, 29.36, 29.31, 28.78, 27.19, 26.98, 23.80, 22.87, and 22.46; IR (KBr) ν 3445, 2918, 2850, and 1703 cm^{-1}; LRMS (ESI) m/z 433.15 (100%, $[M+H]^+$); HRMS (ESI) m/z 433.3788 ($[M+H]^+$, $C_{27}H_{49}N_2O_2^+$ requires 433.3794). Anal. calcd for $C_{27}H_{49}ClN_2O_2 \cdot 2.5H_2O$: C, 63.07; H, 10.59; N, 5.45. Found: C, 63.08; H, 10.51; N, 5.48.

1-(18-(2,5-Dioxo-2,5-dihydro-1*H*-pyrrol-1-yl)octadecyl)pyridinium bromide (PM18). Compound **3b** (50 mg, 0.10 mol) was dissolved in acetone (2 mL), followed by pyridine (81 μL, 1.00 mmol). The resulting mixture was refluxed for 17 hours. Acetone was evaporated in vacuo, the residue was dissolved in anisole (1.0 mL), then refluxed for 15 min. Cooled to room temperature, anisole was evaporated by blowing N_2 to give 51 mg (100%) of **PM18**; mp 94–105°C; ^{1}H NMR (400 MHz, CD_3OD) δ 9.04 (d, J = 5.7 Hz, 2H), 8.61 (t, J = 7.8 Hz, 1H), 8.13 (t, J = 7.0 Hz, 2H), 6.80 (s, 2H), 4.66 (t, J = 7.5 Hz, 2H), 3.47 (t, J = 7.1 Hz, 2H), 2.05–2.01 (m, 2H), 1.57–1.53 (m, 2H), and 1.39–1.27 (m, 28H); ^{13}C NMR (100 MHz, CD_3OD) δ 171.40, 145.68, 144.78, 134.17, 128.33, 61.94, 37.36, 31.37, 29.59, 29.55, 29.48, 29.46, 29.43, 29.34, 29.03, 28.96, 28.33, 26.61, and 26.02; IR (KBr) ν 3055, 2918, 2849, 1703, and 696 cm^{-1}; LRMS (ESI) m/z 427 (100%, $[M]^+$); HRMS m/z 427.3324 ($[M]^+$, $C_{27}H_{43}N_2O_2^+$ requires 427.3325). Anal. calcd for $C_{27}H_{43}BrN_2O_2 \cdot H_2O$: C, 61.70; H, 8.63; N, 5.33. Found: C, 61.85; H, 8.92; N, 5.27.

1-(20-(2,5-Dioxo-2,5-dihydro-1*H*-pyrrol-1-yl)eicosyl)pyridinium bromide (PM20). PM20 was synthesized from **3c** (99% yield) in the same manner as the synthesis of **PM18**; mp 104–112°C ^{1}H NMR (400 MHz, CD_3OD) δ 9.03 (d, J = 6.2Hz, 2H), 8.61 (t, J = 7.8 Hz, 1H), 8.13 (t, J = 6.9 Hz, 2H), 6.80 (s, 2H), 4.65 (t, J = 7.6 Hz, 2H), 3.47 (t, J = 7.1 Hz, 2H), 2.04–2.01 (m, 2H), 1.57–1.53 (m, 2H), and 1.39–1.27 (m, 32H); ^{13}C NMR (100 MHz, CD_3OD) δ 171.40, 145.68, 144.80, 134.16, 128.33, 61.94, 37.35, 31.35, 29.59, 29.55, 29.48, 29.46, 29.43, 29.33, 29.03, 28.95, 28.32, 26.60, and 26.02; IR (KBr) ν 3054, 2918, 2849, 1703, and 696 cm^{-1}; LRMS (EI) m/z 455 (100%, $[M]^+$); HRMS (ESI) m/z 455.3620 ($[M]^+$, $C_{29}H_{47}N_2O_2^+$ requires 455.3638). Anal. calcd for $C_{29}H_{47}BrN_2O_2 \cdot 0.8H_2O$: C, 63.33; H, 8.91; N, 5.09. Found: C, 63.29; H, 9.50; N, 4.98.

1-(18-(Piperidin-1-yl)octadecyl)pyrrolidine-2,5-dione hydrochloride (PYS18). To a round bottom flask equipped with a hydrogen balloon was added **PY18** (10 mg, 0.023 mmol), MeOH (2 mL) and 10% Pd-C (1 mg). The reaction was stirred at room temperature overnight and the catalyst was filtered. The filtrate was evaporated to dryness, leaving a pure product **PYS18** as a white solid (10 mg, 100% yield), mp 112–114°C;^{1}H NMR (400 MHz, $CDCl_3$) δ 11.69 (s, 1H), 3.60–3.45 (s, 2H), 3.48 (t, J = 7.2 Hz, 2H), 2.91 (s, 2H), 2.70 (s, 4H), 2.63 (s, 2H), 2.33 (s, 2H), 1.95–1.80 (m, 6H), 1.60–1.52 (m, 2H), 1.40–1.20 (m, 28H); ^{13}C NMR (100 MHz, $CDCl_3$) δ 177.58, 58.03, 53.54, 39.16, 29.88, 29.86, 29.85, 29.80, 29.79, 29.71, 29.64, 29.40, 29.30, 28.41, 27.95, 27.19, 27.10, 23.77, 22.84, and 22.46; IR (KBr) ν 3434, 2918, 2849, and 1694 cm^{-1}; LRMS (ESI) m/z 435.28 (100%, $[M+H]^+$); HRMS (ESI) m/z 435.3931 ($[M+H]^+$, $C_{27}H_{51}N_2O_2^+$ requires 435.3951). Anal. calcd for $C_{27}H_{51}ClN_2O_2 \cdot 3H_2O$: C, 61.75; H, 10.94; N, 5.33. Found: C, 61.74; H, 10.25; N, 5.02.

1-(20-(2,5-Dioxopyrrolidin-1-yl)eicosyl)pyridin-1-ium 2,2,2-trifluoroacetate (PMS20). To a stirred solution of **PM20** (20 mg, 0.037 mmol) in MeOH (2 mL) was added triphenylphosphine (10.8 mg, 0.041 mmol), the resulting mixture was heated at 75°C for 4 hours. The crude product was purified by HPLC. HPLC conditions: Phenomenex Gemini 5 μ C18 4.6 × 250 mm column, flow rate 1.0 mL/min, solvent A: H_2O + TFA (0.1%), solvent B: MeCN : H_2O = 9 : 1 + TFA (0.1%); linear gradient from 80% A to 0% A over 20 minutes (t_R = 18.40 minutes portion was collected) to give 6 mg (40%) of **PMS20** as a waxy half-solid. ^{1}H NMR (400 MHz, CD_3OD) δ 8.99 (d, J = 5.7 Hz, 2H), 8.60 (t, J = 7.7 Hz, 1H), 8.12 (t, J = 7.0 Hz, 2H), 4.62 (t, J = 7.5 Hz,

2H), 3.45 (t, J = 7.4 Hz, 2H), 2.67 (s, 4H), 2.06–1.96 (m, 2H), 1.57–1.50 (m, 2H), and 1.40–1.24 (m, 32H); ^{13}C NMR (100 MHz, CD_3OD) δ 178.86, 145.67, 144.74, 128.31, 61.93, 38.39, 31.32, 29.58, 29.53, 29.50, 29.44, 29.42, 29.32, 29.09, 28.93, 27.87, 27.46, 26.71, and 26.00; IR (KBr) ν 2919, 2850, 1698, 1205, and 1136 cm^{-1}; LRMS (EI) *m/z* 457 (36%, $[M]^+$); HRMS (ESI) *m/z* 457.3772 ($[M]^+$, $C_{29}H_{49}N_2O_2^+$ requires 457.3794). Anal. calcd for $C_{29}H_{49}N_2O_2^+ \cdot CF_3CO_2^- \cdot CF_3CO_2H \cdot 0.3H_2O$: C, 57.43; H, 7.39; N, 4.06. Found: C, 57.49; H, 7.59; N, 4.35.

Determination of the AChE activity. AChE activity or hydrolysis rate (v) in the absence or presence of an inhibitor at concentrations of ≤30 μM was determined using the Ellman assay[58] through measuring the change in ultraviolet absorbance of an assay solution at 405 nm over a period of 2 minutes at 25°C with a SpectraMax Plus 384 Absorbance Microplate Reader from Molecular Devices (Sunnyvale, CA). Justification for the use of the Ellman assay to test sulfhydryl agents is provided in the Supplementary Information.

Determination of irreversible inhibition through dilution. In a typical dilution experiment with a 96-well plate, to 300 μL of 50 mM phosphate buffer (pH 8.0) was added 3 μL of 2 μg/mL agAP-AChE or 1 μg/mL hAChE, and then 5 μL of neat dimethyl sulfoxide (DMSO) or an inhibitor in neat DMSO freshly prepared at a concentration leading to ~50% enzyme inhibition using a 10 μL Eppendorf Research plus pipette. The resulting solution was mixed through 10 repetitions of uptake and expulsion of part of the solution using the pipette while moving the pipette tip around the bottom of the well. The solution was then incubated for 30 minutes at 25°C. At the end of incubation, a 50 μL Eppendorf Research plus pipette was used to transfer 28 μL of the solution to a well preloaded with 252 μL of 50 mM phosphate buffer (pH 8.0), and the resulting solution was mixed with the pipette. To the original and diluted enzyme solutions were added sequentially 10 μL of 2.5 mM DTNB and 10 μL of 30 mM ATCh. The resulting solution was quickly mixed with the pipette and measured immediately for v. Each dilution experiment was performed in triplicates. The AChE inhibition was determined by calculating the difference of v in the presence and absence of a test inhibitor. The irreversible AChE inhibition was determined by the null effect of the dilution on the AChE inhibition.

Determination of k_{inact} and K_I. To each well containing 270 μL of 50 mM phosphate buffer (pH 8.0) and 5 μL of 1 μg/mL agAP-AChE or 0.5 μg/mL hAChE was added 5 μL of DMSO as a control or an inhibitor in neat DMSO freshly prepared at varying concentrations, using a 10 μL Eppendorf Research plus pipette. The resulting solution was mixed with the pipette. To the control solution was added 10 μL of 2.5 mM DTNB and 10 μL of 30 mM ATCh. The resulting solution was quickly mixed with the pipette and measured immediately for v_0. Each of the inhibitor-containing solutions was incubated for various amounts of time at 25°C. At the end of the incubation, to the incubation solution was added 10 μL of 2.5 mM DTNB and 10 μL of 30 mM ATCh. The resulting solution was quickly mixed with the pipette and measured immediately for v. The k_{obs} value was obtained from the slope of the line of $\ln(v/v_0)$ versus time according to Equation 1 in Figure 1 using GraphPad Prism Version 5.0d for Mac OS X from GraphPad Software (San Diego, CA). Linear fitting was used and the lines were forced to go through x = 0 and y = 0. Each of the k_{obs} values used for the subsequent k_{inact} and K_I determination was an average of two independent experiments. The k_{inact} and K_I values were then computed from the curve of k_{obs} versus the associated [I] according to Equation 2 in Figure 1 using Prism 4 with nonlinear fitting.

Determination of K_i. To each well was added sequentially 270 μL of 50 mM phosphate buffer (pH 8), 5 μL of 1 μg/mL agAP-AChE or 0.5 μg/mL of hAChE, 5 μL of DMSO or an inhibitor in neat DMSO freshly prepared at varying concentrations, 10 μL of 2.5 mM DTNB, and 10 μL of 0.9375, 1.25, 1.875, 3.75, 7.5, or 15 mM ATCh. The resulting solutions were mixed with a 1–10 μL multichannel pipette from Thermo Fisher Scientific and measured immediately for v. K_i was then obtained from 1/v, 1/[ATCh], and [I] using Prism 4 with the Lineweaver-Burk plot[59].

Liquid chromatography tandem mass spectrometric detection of the PM20 adduct. To agAP-AChE (100 ng) in 21 μL of 50 mM phosphate buffer (pH 8.0) was added 0.5 μL of 10 mM **PM20** in neat DMSO and the solution was incubated at room temperature for 1 hour. After enzyme activity and its complete loss before and after the incubation were confirmed, the sample was added to 4x sodium dodecyl sulfate polyacrylamide gel electrophoresis (SDS-PAGE) loading buffer (200 mM Tris buffer, pH 6.8, 400 mM dithiothreitol, 8% SDS, and 40% glycerol) and heated to 100°C for 5 minutes. The sample was then loaded on a 4–20% gradient SDS-PAGE gel and run under 100 volts for 90 minutes. After the silver-stained SDS-PAGE gel band of the agAP-AChE was destained with potassium ferricyanide and sodium thiosulfate according to a published protocol[60], the gel band containing agAP-AChE was cut into small pieces and treated with 50 mM tris(2-carboxyethyl)phosphine in 50 mM Tris buffer (pH 8.1) at 55°C for 40 minutes then alkylated with 40 mM iodoacetamide at room temperature for 40 minutes in the dark. The protein was digested in situ with 0.15 μg chymotrypsin from Roche (Indianapolis, IN) in 25 mM Tris buffer (pH 8.1) with 0.0002% Zwittergent 3–16 at room temperature overnight followed by peptide extraction with 2% trifluoroacetic acid and then with acetonitrile. The pooled extracts were concentrated to <5 μL on a SpeedVac spinning concentrator from Savant Instruments (Holbrook, NY) and then brought up in 0.2% trifluoroacetic acid for peptide identification using a ThermoFinnigan LTQ Orbitrap hybrid mass spectrometer from Thermo Fisher Scientific coupled to a nano-scale, two-dimensional high-performance liquid chromatography system from Eksigent. The solution of the digested peptides of agAP-AChE was loaded onto a 250-nL OPTI-PAK trap from Optimize Technologies (Oregon City, OR) custom packed with Michrom Magic C8 solid phase (Michrom Bioresources, Auburn, CA). Chromatography was performed using 0.2% formic acid in both the A solvent (98% water with 2% acetonitrile) and the B solvent (80% acetonitrile with 10% isopropanol and 10% water) and a 5% B to 50% B gradient over 35 minutes at 325 nL/min through a hand packed PicoFrit from New Objective (Woburn, MA) 75 μm × 100-mm column (Michrom Magic C18 3 μm). The LTQ Orbitrap tandem mass spectrometer was set to perform a Fourier transform full scan from *m/z* 350–1450 with resolution at 60,000 (400 *m/z*) followed by linear ion trap MS/MS scans on the top five ions. Dynamic exclusion was set to 1 and selected ions were placed on an exclusion list for 15 seconds. The lock-mass option was enabled for the Fourier transform full scans using the ambient air polydimethylcyclosiloxane ion with *m/z* 445.120024 or a common phthalate ion with *m/z* 391.284286 for real-time internal calibration. ChemDraw Ultra Version 12.0.3.1216 from CambridgeSoft (Cambridge, MA) was used to calculate the *m/z* values for the identified agAP-AChE fragments. Tandem mass spectra were extracted using BioWorks version 3.2 and analyzed using Sequest from ThermoFinnigan (San Jose, CA). Sequest was searched with a fragment ion mass tolerance of 0.60 and a parent ion tolerance of 25 ppm. Oxidation of methionine and iodoacetamide derivative of cysteine were specified as variable modifications in addition to the modification by the conjugation of **PM20**.

1. Miller, L. H., Baruch, D. I., Marsh, K. & Doumbo, O. K. The pathogenic basis of malaria. *Nature* **415**, 673–679 (2002).
2. Joy, D. A. *et al.* Early origin and recent expansion of Plasmodium falciparum. *Science* **300**, 318–321 (2003).
3. Sachs, J. & Malaney, P. The economic and social burden of malaria. *Nature* **415**, 680–685 (2002).
4. World Malaria Report 2011. http://www.who.int/malaria/world_malaria_report_2011/9789241564403_eng.pdf Accessed August 31, 2012.
5. Fialka, J. J. EPA scientists cite pressure in pesticide study. *Wall Street Journal,* A4 (May 25, 2006).
6. Weill, M. *et al.* Comparative genomics: Insecticide resistance in mosquito vectors. *Nature* **423**, 136–137 (2003).
7. Hamer, G. L. *et al.* Host selection by *Culex pipiens* mosquitoes and West Nile virus amplification. *Am. J. Trop. Med. Hyg.* **80**, 268–278 (2009).
8. Sussman, J. L. *et al.* Atomic structure of acetylcholinesterase from *Torpedo californica*: a prototypic acetylcholine-binding protein. *Science* **253**, 872–879 (1991).
9. Taylor, P. & Radic, Z. The cholinesterases: from genes to proteins. *Ann. Rev. Pharmacol.* **34**, 281–320 (1994).
10. Raves, M. L. *et al.* Structure of acetylcholinesterase complexed with the nootropic alkaloid, (-)-huperzine A. *Nat. Struct. Biol.* **4**, 57–63 (1997).
11. Pang, Y.-P., Brimijoin, S., Ragsdale, D. W., Zhu, K. Y. & Suranyi, R. Novel and viable acetylcholinesterase target site for developing effective and environmentally safe insecticides. *Curr. Drug Targets* **13**, 471–482 (2012).
12. Pang, Y.-P. *et al.* Selective and irreversible inhibitors of aphid acetylcholinesterases: steps toward human-safe insecticides. *PLoS One* **4**, e4349 (2009).
13. Lu, Y. *et al.* Genome organization, phylogenies, expression patterns, and three-dimensional protein models of two acetylcholinesterase genes from the red flour beetle. *PLoS One* **7**, e32288 (2012).
14. Lu, Y. *et al.* Cholinergic and non-cholinergic functions of two acetylcholinesterase genes revealed by gene-silencing in *Tribolium castaneum*. *Sci. Rep.* **2**, 288 (2012).
15. Pang, Y.-P. *et al.* Selective and irreversible inhibitors of mosquito acetylcholinesterases for controlling malaria and other mosquito-borne diseases. *PLoS One* **4**, e6851 (2009).
16. Jennings, L. L., Malecki, M., Komives, E. A. & Taylor, P. Direct analysis of the kinetic profiles of organophosphate-acetylcholinesterase adducts by MALDI-TOF mass spectrometry. *Biochemistry* **42**, 11083–11091 (2003).
17. Tsuge, K. & Seto, Y. Detection of human butyrylcholinesterase-nerve gas adducts by liquid chromatography-mass spectrometric analysis after in gel chymotryptic digestion. *J. Chromatogr. B Analyt. Technol. Biomed. Life Sci.* **838**, 21–30 (2006).
18. Ekström, F. J., Astot, C. & Pang, Y.-P. Novel nerve-agent antidote design based on crystallographic and mass spectrometric analyses of tabun-conjugated acetylcholinesterase in complex with antidotes. *Clin. Pharmacol. Ther.* **82**, 282–293 (2007).
19. Carletti, E. *et al.* Aging of cholinesterases phosphylated by tabun proceeds through O-dealkylation. *J. Am. Chem. Soc.* **130**, 16011–16020 (2008).
20. Dutta, S., Malla, R. K., Bandyopadhyay, S., Spilling, C. D. & Dupureur, C. M. Synthesis and kinetic analysis of some phosphonate analogs of cyclophostin as inhibitors of human acetylcholinesterase. *Bioorg. Med. Chem.* **18**, 2265–2274 (2010).
21. Carletti, E. *et al.* Reaction of cresyl saligenin phosphate, the organophosphorus agent implicated in aerotoxic syndrome, with human cholinesterases: mechanistic studies employing kinetics, mass spectrometry, and x-ray structure analysis. *Chem. Res. Toxicol.* **24**, 797–808 (2011).
22. Aryal, U. K. *et al.* Identification of phosphorylated butyrylcholinesterase in human plasma using immunoaffinity purification and mass spectrometry. *Anal. Chim. Acta* **723**, 68–75 (2012).

23. Jiang, H., Liu, S., Zhao, P. & Pope, C. Recombinant expression and biochemical characterization of the catalytic domain of acetylcholinesterase-1 from the African malaria mosquito, Anopheles gambiae. *Insect Biochem. Mol. Biol.* **39**, 646–653 (2009).
24. Pang, Y.-P. Novel acetylcholinesterase target site for malaria mosquito control. *PLoS One* **1**, e58 (2006).
25. Zauhar, R. J., Colbert, C. L., Morgan, R. S. & Welsh, W. J. Evidence for a strong sulfur-aromatic interaction derived from crystallographic data. *Biopolymers* **53**, 233–248 (2000).
26. Copeland, R. A. *Evaluation of enzyme inhibitors in drug discovery: a guide for medicinal chemists and pharmacologists.* (John Wiley & Sons, 2005).
27. Wilson, I. B., Ginsburg, S. & Quan, C. Molecular complementariness as basis for reactivation of alkyl phosphate-inhibited enzyme. *Arch. Biochem.* **77**, 286–296 (1958).
28. Jorgensen, W. L., Chandreskhar, J., Madura, J. D., Impey, R. W. & Klein, M. L. Comparison of simple potential functions for simulating liquid water. *J. Chem. Phys.* **79**, 926–935 (1982).
29. Pang, Y.-P. Three-dimensional model of a substrate-bound SARS chymotrypsin-like cysteine proteinase predicted by multiple molecular dynamics simulations: catalytic efficiency regulated by substrate binding. *Proteins.* **57**, 747–757 (2004).
30. Pang, Y.-P. *et al.* Bak Conformational Changes Induced by Ligand Binding: Insight into BH3 Domain Binding and Bak Homo-Oligomerization. *Sci. Rep.* **2**, 257 (2012).
31. Clevenger, R. C. & Turnbull, K. D. Synthesis on N-alkylated maleimides. *Synth. Commun.* **30**, 1379–1388 (2000).
32. Pang, Y.-P. *et al.* Discovery of a new inhibitor lead of adenovirus proteinase: steps toward selective, irreversible inhibitors of cysteine proteinases. *FEBS Lett.* **502**, 93–97 (2001).
33. Olsen, J. V. *et al.* Parts per million mass accuracy on an Orbitrap mass spectrometer via lock mass injection into a C-trap. *Mol. Cell. Proteomics* **4**, 2010–2021 (2005).
34. Mather, B. D., Viswanathan, K., Miller, K. M. & Long, T. E. Michael addition reactions in macromolecular design for emerging technologies. *Prog. Polym. Sci.* **31**, 487–531 (2006).
35. Roepstorff, P. & Fohlman, J. Proposal for a common nomenclature for sequence ions in mass spectra of peptides. *Biomed. Mass Spectrom.* **11**, 601 (1984).
36. Yalcin, T., Csizmadia, I. G., Peterson, M. R. & Harrison, A. G. The structure and fragmentation of Bn ($n \geq 3$) ions in peptide spectra. *J. Am. Soc. Mass. Spectrom.* **7**, 233–242 (1996).
37. Oomens, J., Young, S., Molesworth, S. & Van Stipdonk, M. Spectroscopic evidence for an oxazolone structure of the b(2) fragment ion from protonated tri-alanine. *J. Am. Soc. Mass. Spectrom.* **20**, 334–339 (2009).
38. Yoon, S. H. *et al.* IRMPD spectroscopy shows that AGG forms an oxazolone b2+ ion. *J. Am. Chem. Soc.* **130**, 17644–17645 (2008).
39. Bythell, B. J., Erlekam, U., Paizs, B. & Maître, P. Infrared spectroscopy of fragments from doubly protonated tryptic peptides. *Chem Phys Chem* **10**, 883–885 (2009).
40. Chen, X., Yu, L., Steill, J. D., Oomens, J. & Polfer, N. C. Effect of peptide fragment size on the propensity of cyclization in collision-induced dissociation: oligoglycine b(2)–b(8). *J. Am. Chem. Soc.* **131**, 18272–18282 (2009).
41. Polfer, N. C., Oomens, J., Suhai, S. & Paizs, B. Spectroscopic and theoretical evidence for oxazolone ring formation in collision-induced dissociation of peptides. *J. Am. Chem. Soc.* **127**, 17154–17155 (2005).
42. Harrison, A. G., Young, A. B., Bleiholder, C., Suhai, S. & Paizs, B. Scrambling of sequence information in collision-induced dissociation of peptides. *J. Am. Chem. Soc.* **128**, 10364–10365 (2006).
43. Riba-Garcia, I., Giles, K., Bateman, R. H. & Gaskell, S. J. Evidence for structural variants of a- and b-type peptide fragment ions using combined ion mobility/mass spectrometry. *J. Am. Soc. Mass. Spectrom.* **19**, 609–613 (2008).
44. Jia, C., Qi, W. & He, Z. Cyclization reaction of peptide fragment ions during multistage collisionally activated decomposition: an inducement to lose internal amino-acid residues. *J. Am. Soc. Mass. Spectrom.* **18**, 663-678 (2007).
45. Molesworth, S., Osburn, S. & Van Stipdonk, M. Influence of size on apparent scrambling of sequence during CID of b-type ions. *J. Am. Soc. Mass. Spectrom.* **20**, 2174–2181 (2009).
46. Harrison, A. G. Cyclization of peptide b9 ions. *J. Am. Soc. Mass. Spectrom.* **20**, 2248–2253 (2009).
47. Erlekam, U. *et al.* Infrared spectroscopy of fragments of protonated peptides: direct evidence for macrocyclic structures of b5 ions. *J. Am. Chem. Soc.* **131**, 11503–11508 (2009).
48. Wong, S. S. & Jameson, D. M. *Chemistry of protein and nucleic acid cross-linking and conjugation* Second edn (CRC Press, 2012).
49. Brewer, C. F. & Riehm, J. P. Evidence for possible nonspecific reactions between N-ethylmaleimide and proteins. *Anal. Biochem.* **18**, 248–255 (1967).
50. Maurer, T. & Fung, H. L. Comparison of methods for analyzing kinetic data from mechanism-based enzyme inactivation: application to nitric oxide synthase. *AAPS Pharm Sci* **2**, E8 (2000).
51. Kardos, S. A. & Sultatos, L. G. Interactions of the organophosphates paraoxon and methyl paraoxon with mouse brain acetylcholinesterase. *Toxicol. Sci.* **58**, 118–126 (2000).
52. Kousba, A. A., Sultatos, L. G., Poet, T. S. & Timchalk, C. Comparison of chlorpyrifos-oxon and paraoxon acetylcholinesterase inhibition dynamics: potential role of a peripheral binding site. *Toxicol. Sci.* **80**, 239–248 (2004).
53. Rosenfeld, C. A. & Sultatos, L. G. Concentration-dependent kinetics of acetylcholinesterase inhibition by the organophosphate paraoxon. *Toxicol. Sci.* **90**, 460–469 (2006).
54. Wang, C. & Murphy, S. D. Kinetic analysis of species difference in acetylcholinesterase sensitivity to organophosphate insecticides. *Toxicol. Appl. Pharm.* **66**, 409–419 (1982).
55. Amitai, G., Moorad, D., Adani, R. & Doctor, B. P. Inhibition of acetylcholinesterase and butyrylcholinesterase by chlorpyrifos-oxon. *Biochem. Pharmacol.* **56**, 293–299 (1998).
56. Krasinski, A. *et al.* In situ selection of lead compounds by click chemistry: target-guided optimization of acetylcholinesterase inhibitors. *J. Am. Chem. Soc.* **127**, 6686–6692 (2005).
57. Beck, A., Heissler, D. & Duportail, G. Synthesis of fluorescent probes for localized membrane fluidity measurements. *Tetrahedron* **47**, 1459–1472 (1991).
58. Ellman, G. L., Courtney, K. D., Andres, V. J. & Featherstone, R. M. A new and rapid colorimetric determination of acetylcholinesterase activity. *Biochem. Pharmacol.* **7**, 88–95 (1961).
59. Lineweaver, H. & Burk, D. The determination of enzyme dissociation constants. *J. Am. Chem. Soc.* **56**, 658–666 (1934).
60. Gharahdaghi, F., Weinberg, C. R., Meagher, D. A., Imai, B. S. & Mische, S. M. Mass spectrometric identification of proteins from silver-stained polyacrylamide gel: a method for the removal of silver ions to enhance sensitivity. *Electrophoresis* **20**, 601–605 (1999).

Acknowledgement

This work was supported by the U.S. Department of Agriculture (2010-65105-20553 to Y.-P.P.) and in part by the University of Minnesota Supercomputing Institute for the computational study.

Author contributions

Y.-P.P. conceived, designed, and supervised the project. Y.-P.P. and J.G.P. designed **PYn**, **PMn**, **PYS18** and **PMS20**. Y.-P.P. performed the computational study. D.D. first synthesized **PYn**; S.R. then synthesized **PMn**; J.G.P. subsequently developed the improved synthetic scheme for **PYn**, **PMn**, **PYS18** and **PMS20** shown in Figure 1. D.D. designed the experiment shown in Figure 7, established the kinetics study protocols, and performed the kinetics studies. B.J.M. and D.D. designed and performed the nanoLC-ESI-MS/MS study. Y.-P.P., D.D., J.G.P., S.R. and B.J.M. analyzed the data. H.J. made the recombinant agAP-AChE. Y.-P.P. wrote the paper; D.D., J.G.P., S.R. and B.J.M. drafted parts of the methods section; Y.-P.P., D.D., J.G.P., S.R. and B.J.M. contributed with revisions.

Additional information

Supplementary information accompanies this paper at http://www.nature.com/scientificreports

Competing financial interests: Y.-P.P., D.D., J.G.P. and S.R. are inventors of a filed patent application that covers the inhibitors disclosed in this article.

How to cite this article: Dou, D. *et al.* Novel Selective and Irreversible Mosquito Acetylcholinesterase Inhibitors for Controlling Malaria and Other Mosquito-Borne Diseases. *Sci. Rep.* **3**, 1068; DOI:10.1038/srep01068 (2013).